Visualization of tRNA Movements on the *Escherichia coli* 70S Ribosome During the Elongation Cycle

Rajendra K. Agrawal,* Christian M.T. Spahn,‡‖ Pawel Penczek,* Robert A. Grassucci,‡ Knud H. Nierhaus,‖ and Joachim Frank*‡

*Wadsworth Center, Department of Biomedical Sciences, State University of New York, Albany, New York 12201; ‡Howard Hughes Medical Institute, Health Research, Incorporated at Wadsworth Center, Albany, New York 12201; and ‖Max-Planck-Institut für Molekulare Genetik, Ihnestrasse 73, D-14195 Berlin, Germany

Abstract. Three-dimensional cryomaps have been reconstructed for tRNA–ribosome complexes in pre- and posttranslocational states at 17-Å resolution. The positions of tRNAs in the A and P sites in the pretranslocational complexes and in the P and E sites in the posttranslocational complexes have been determined. Of these, the P-site tRNA position is the same as seen earlier in the initiation-like fMet-$tRNA_f^{Met}$-ribosome complex, where it was visualized with high accuracy. Now, the positions of the A- and E-site tRNAs are determined with similar accuracy. The positions of the CCA end of the tRNAs at the A site are different before and after peptide bond formation. The relative positions of anticodons of P- and E-site tRNAs in the posttranslocational state are such that a codon–anticodon interaction at the E site appears feasible.

Key words: ribosomes • protein synthesis • tRNA-binding sites • cryoelectron microscopy • elongation cycle

Introduction

The ribosome conducts the biosynthesis of the polypeptide chain according to the genetic code of the mRNA. Addition of each amino acid and peptide bond formation entails a cycle, the elongation cycle, of several binding and interaction events between the ribosome, the mRNA, and tRNA, which carries the covalently bound amino acid. During the cycle, the tRNA occupies successive positions on the ribosome (for reviews, see Spahn and Nierhaus, 1998; Wilson and Noller, 1998). It first enters the A site as an aminoacyl-tRNA, then, after the peptide bond formation, it moves to the P site as a peptidyl tRNA, and finally to the E site as a deacylated tRNA before leaving the ribosome. Pretranslocational (PRE)[1] and posttranslocational (POST) states constitute the two main conformational and functional states of the ribosome within the elongation cycle. A and P sites are occupied in the PRE state, whereas P and E sites are occupied, after elongation factor G (EF-G)–dependent translocation, in the POST state. In addition to the three principal, A, P, and E sites on the ribosome, evidence suggesting two additional intermediate binding states, A/P and P/E (Moazed and Noller, 1989a), and more than one E site-related binding positions (Lill et al., 1986; Robertson et al., 1986) led to the proposal that several (seven or more) tRNA-binding positions might be assumed on the ribosome (Green and Noller, 1997).

Knowledge of three-dimensional (3D) binding positions of tRNAs, in the course of the elongation cycle, is crucial for an understanding of the mechanism of protein biosynthesis. In the past, extensive efforts have been made to determine the tRNA positions on the ribosome by interpretation of the cross-linking experiments between specific nucleotides of tRNA and various components of the ribosome, i.e., ribosomal proteins or specific nucleotides of ribosomal RNA (e.g., see Brimacombe, 1995), whose positions in some instances are tentatively known from immunoelectron microscopy (Stöffler-Meilicke and Stöffler, 1990). Obviously, the tRNA positions derived from such cross-linking experiments (for review see Wower et al., 1993; for an updated summary of cross-linking data see Nagano and Nagano, 1997) had to remain tentative in the absence of structural data.

In the last five years, significant progress has been made in the structural studies of ribosomes (reviews by Agrawal and Frank, 1999; Green and Puglisi, 1999). Particularly, 3D cryoelectron microscopy (cryo-EM) has been extremely useful in investigating the interactions of various ligands with the *Escherichia coli* 70S ribosome by visualizing tRNAs, in

Address correspondence to Joachim Frank, HHMI, Wadsworth Center, Empire State Plaza, PO Box 509, Albany, NY 12201-0509. Tel.: 518 474-7002. Fax: 518 486-2191. E-mail: joachim@wadsworth.org

[1]*Abbreviations used in this paper:* 3D, three-dimensional; ASL, anticodon stem-loop; cryo-EM, cryoelectron microscopy; EF-G, elongation factor G; EF-Tu, elongation factor Tu; MF-mRNA, 46-nt long mRNA with AUG and UUC codon in its middle; POST, posttranslocational; PRE, pretranslocational.

different tRNA–ribosome complexes existing in well-characterized functional states (Agrawal et al., 1996, 1999a,c; Stark et al., 1997a; see review by Frank, 1998; Malhotra et al., 1998), and elongation factors Tu (EF-Tu; Stark et al., 1997b; Agrawal et al., 2000) and EF-G (Agrawal et al., 1998, 1999a, 2000).

With the exception of the position of the P-site tRNA, which was determined with high accuracy in maps of the *E. coli* 70S–fMet-tRNA$_f^{Met}$ complex at 15 Å (Malhotra et al., 1998), and at 11.5-Å (Gabashvili et al., 2000) resolution, the resolution of various cryo-EM maps has been generally insufficient to determine unambiguously the position of tRNA at the different sites of the ribosome during the elongation cycle. On the other hand, some experiments have given clear indication that the tRNA positions vary significantly with the buffer conditions (Agrawal et al., 1999c), and with the aminoacylated and deacylated state of the tRNA (Agrawal et al., 1996, 1999c; Malhotra et al., 1998). Recently, the binding position of A-, P-, and E-site tRNAs were also derived, at 7.8-Å resolution, by X-ray crystallography (Cate et al., 1999) of *Thermus thermophilus* 70S–tRNA and 70S–anticodon stem-loop (ASL) complexes, which were prepared under nonphysiological conditions (see Discussion). Thus, even though great progress has been made in visualizing tRNA bound to the ribosome, the binding positions in functionally relevant PRE and POST states have remained uncertain. Examples of the remaining questions are the orientation of the A-site tRNA in the PRE state, the relationship between the P site position in the POST state and the position found for fMet-tRNA$_f^{Met}$, and the relationship between the E-site tRNA positions found by two groups (Agrawal et al., 1996; Stark et al., 1997a).

To determine the tRNA positions with greater accuracy, we have obtained 3D cryo-EM maps of tRNA–ribosome complexes in PRE and POST states in precisely controlled conditions, at a significantly improved resolution of 17 Å (or ~13 Å, using the 3σ criterion; Orlova et al., 1997; but see Materials and Methods). So far, we have inferred six different tRNA locations, termed A (before peptide bond formation), A$_{Pep}$ (after peptide bond formation), P, P/E, E, and E2, from the analysis of these complexes, as well as complexes analysed in our previous studies (Agrawal et al., 1996, 1999a,c; Malhotra et al., 1998; Gabashvili et al., 2000). Taken together, these results have enabled us to deduce the principal positions that tRNA assumes in the course of the elongation cycle.

Materials and Methods

Preparation of tRNA–Ribosome Complexes

PRE and POST complexes were prepared by using the ribosomes isolated by the method of Bommer et al. (1997). These complexes were prepared using low Mg^{2+} containing polyamine buffer (20 mM Hepes/KOH, 6 mM $Mg(CH_3COO)_2$, 150 mM NH_4Cl, 4 mM mercaptoethanol, 0.05 mM spermine, 2 mM spermidine). Ribosomes programmed with MF-mRNA were incubated with 1.7-M excess of fMet-tRNA$_f^{Met}$ and were then incubated with 2-M excess of EF-Tu–Phe-tRNA^{Phe}–GTP. A spontaneous peptide bond formation, induced by peptidyltransferase activity of the 50S subunit takes place between the amino acids of A- and P-site tRNA. As a result, the PRE complex contained tRNA$_f^{Met}$ at the P site and fMet-Phe-tRNA^{Phe} at the A site. To prevent excessive spontaneous translocation, the incubation was carried out at 20°C for 5 min. This complex was divided into two parts and one part was incubated with EF-G for 10 min at 37°C to establish the POST state. Thus, the posttranslocation complex contained tRNA$_f^{Met}$ at the E site and Met-Phe-tRNA^{Phe} at the P site. Approximately 90% of the Phe-tRNA^{Phe} was located at the A site of the PRE complex as determined by the puromycin reaction (Bommer et al., 1997). The P site location of the fMet-Phe-tRNA^{Phe} of the POST complex was >90%.

Electron Microscopy and Image Processing

In each case, samples were diluted in the corresponding buffers to a concentration of 1.3 A_{260}/ml. Grids were prepared for cryo-EM according to standard methods (Dubochet et al., 1988; Wagenknecht et al., 1988). Micrographs were recorded using low-dose protocols on a Philips EM420, equipped with low-dose kit and a GATAN (model/626) cryotransfer holder, at 52,200× ± 2% as checked by a tobacco mosaic virus standard. Each exposure corresponds to an electron dose of ~10 e^-/A^2. Micrographs were checked for drift, astigmatism, and presence of Thon rings by optical diffraction. Scanning was done with a step size of 25 μm corresponding to 4.78 Å on the object scale, on a PDS 1010A microdensitometer (Perkin Elmer) and on a Hi-Scan drum scanner (Eurocore). 3D reconstructions were calculated and refined using the 3D projection alignment procedure (Penczek et al., 1994), and were CTF-corrected as described earlier (Zhu et al., 1997). 15,610 and 18,341 particles covering several defocus settings in each case were used to obtain the 3D maps of PRE and POST complexes, respectively. The final resolution was estimated using the Fourier shell correlation with a threshold of 0.5 (see Malhotra et al., 1998). The values found were 17 Å and 16.7 Å for the PRE and POST complexes, respectively. If we use the 3σ criterion for measuring resolution (Orlova et al., 1997), the values are 12.8 Å and 12.9 Å for PRE and POST complexes, respectively. However, inclusion of information beyond 17 Å into final map is not justified as the signal-to-noise ratio falls below 1 (see Malhotra et al., 1998). High spatial frequency components were enhanced by applying a correction to the Fourier amplitudes based on X-ray solution scattering measurements for the *E. coli* ribosome (Gabashvili et al., 2000). Difference maps were computed by subtracting the 3D maps fMet-tRNA$_f^{Met}$-ribosome complex (Malhotra et al., 1998; Agrawal et al., 1999c) in the corresponding buffers (see Figs. 2 and 3).

Protein Data Bank Identification

The coordinates of the tRNA in the A, A$_{pep}$, P, E, and E$_2$ positions obtained in this study have been deposited in the Protein Data Bank (code #IFCW).

Results

3D cryo-EM maps of two tRNA–ribosome complexes, PRE and POST, were obtained in this study. Three principal tRNA-binding positions, in A, P, and E sites, were derived directly from the 3D maps. In contrast, the positions of tRNA in binding states with low occupancy were derived by computation of difference maps between the 3D cryo-maps of a tRNA–ribosome complex and a suitable control.

Analysis of the PRE and POST Complexes

Two PRE complexes were analyzed in the present study: one prepared by the binding of a deacylated tRNA^{Phe} at the P site and a Phe-tRNA^{Phe} at the A site on a poly (U)-programmed 70S ribosome (Fig. 1 a; see Agrawal et al., 1999a); and the other prepared (see Materials and Methods) by binding of an fMet-tRNA$_f^{Met}$ at the P site and Phe-tRNA^{Phe} at the A site, in a codon-dependent manner, of the 70S ribosome programmed with MF-mRNA (a 46-nt mRNA fragment that carries unique AUG and UUC codons in its middle; Triana-Alonso et al., 1995). In the latter case, a spontaneous peptidyltransferase reaction results in a dipeptidyl-tRNA (fMet-Phe-tRNA^{Phe}) at the A site and a deacylated tRNA$_f^{Met}$ at the P site.

The POST complexes were obtained by EF-G–dependent translocation of the PRE complexes. One POST complex is expected to contain Phe-tRNA^{Phe} at the P site and a deacy-

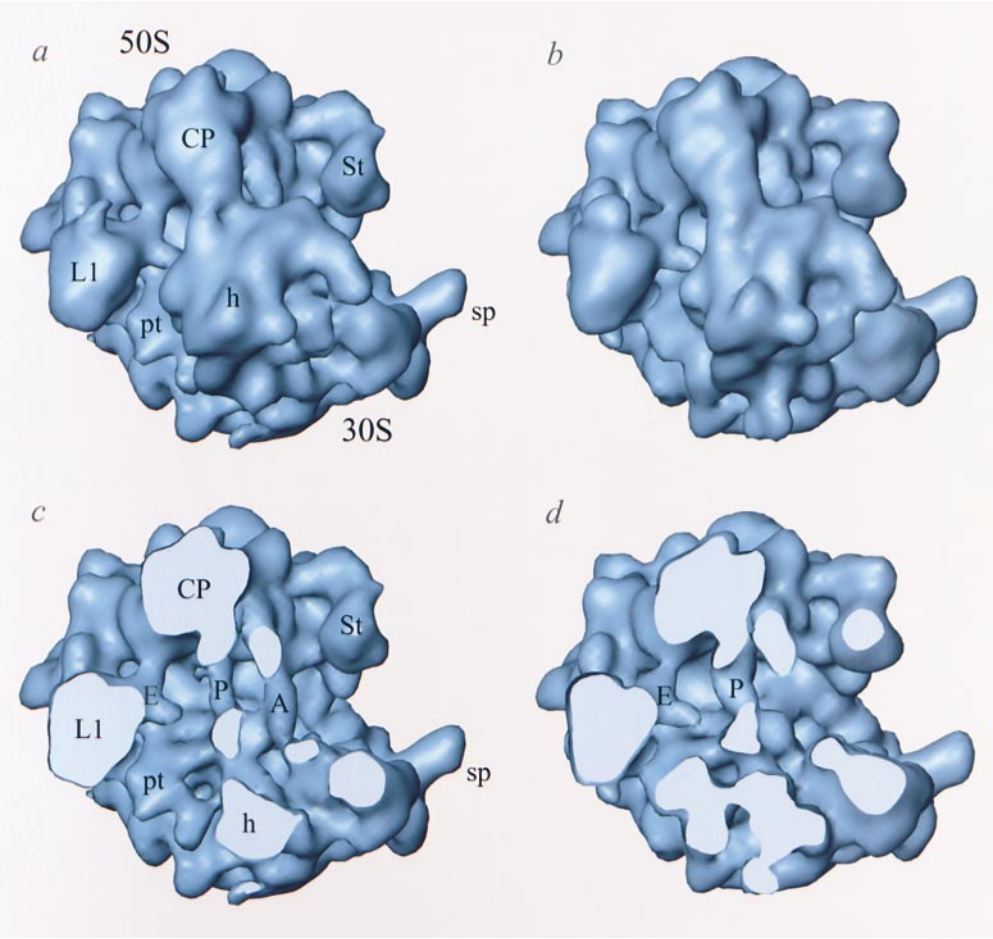

Figure 1. 3D maps of the PRE (a; with Phe-tRNA^{Phe} at the A site) and the POST (b; with dipeptidyl tRNA at the P site) complexes shown in top view, with the 30S subunit below the 50S subunit. c and d, The ribosome cut open, by removing the portions of head and central protuberance of the 30S and the 50S subunits, respectively, to expose the intersubunit space where tRNAs bind. The A-, P-, and E-site tRNA masses can be seen directly. c, The PRE complex as shown in a. d, The POST complex as shown in b. The PRE complex also shows an unexpected mass corresponding to the E-site tRNA on the L1 protein side, which is due to the binding of deacylated tRNA in a fraction of PRE complex. CP, central protuberance; L1, L1 protein; St, L7/L12-stalk base, where protein L11 complexed with 58-nt 23S RNA fragment has been located in an earlier study (Gabashvili et al., 2000); h, head; pt, platform; sp, spur.

lated tRNA^{Phe} at the E site (Agrawal et al., 1999a), whereas another POST complex is expected to contain a dipeptidyl-tRNA (fMet-Phe-tRNA^{Phe}) at the P site and a deacylated tRNA$_f^{Met}$ at the E site (Fig. 1 b). Whereas the P and E site locations of tRNAs could be inferred directly from the 3D maps of both POST complexes, the A site location could be inferred directly only from one of the PRE complexes, in which Phe-tRNA^{Phe} was bound to poly(U)-programmed ribosome (Fig. 1 c). Thus, in three complexes (one PRE and both POSTs), tRNA densities are clearly visible. It should be pointed out that in the PRE complexes, a density is also seen in the L1 protein region (Fig. 1 c), which appears to be due to the binding of deacylated tRNAs in the E site region, or represents density from a fraction of complex that has undergone spontaneous translocation. The reason why the tRNA is seen directly in the A site of the PRE complex containing Phe-tRNA^{Phe} and not in the PRE complex containing dipeptidyl-tRNA, could be due to the fact that spontaneous translocation is favored after the peptide bond formation (Bergemann and Nierhaus, 1983), which is the situation in the latter case. Since the density corresponding to the A-site tRNA in the PRE complex containing dipeptidyl-tRNA (fMet-Phe-tRNA^{Phe}) at the A site was not directly visible, a difference map was calculated.

Computation of the Difference Maps

One of the difficulties of the study is the choice of the control in the computation of difference maps. In the very first visualization of tRNA positions (Agrawal et al., 1996), we used the vacant ribosome as control. In the subsequent study of the fMet-tRNA$_f^{Met}$–ribosome complex (Malhotra et al., 1998), some conformational changes were observed in the ribosome as compared with the vacant ribosome, which could have been due to either the initial binding of mRNA, or tRNA, or both. These conformational changes showed a general positional consistency in other tRNA–ribosome complexes as well (see Agrawal et al., 1999b). The vacant ribosome is known to be present in at least two conformational states (Ghosh and Moore, 1979; Mesters et al., 1994; Agrawal and Burma, 1996), and thus it was realized that a reconstruction from such a specimen was not well suited as a control for computing the difference maps in experiments where distinct functional complexes are visualized. Moreover, the binding of the first tRNA to a programmed ribosome requires an activation energy of ~40 kJ/mol (Schilling-Bartetzko et al., 1992), indicative of a conformational change of the ribosome. Structural changes were indeed found in the regions of the L1 protein and the central protuberance (Agrawal et al., 1999b). Therefore, the 3D map of the fMet-tRNA$_f^{Met}$–ribosome complex, the conformation of which was expected to be closer to that of elongating ribosomes, was used as a control in the present study to determine difference maps. This approach was a major help in the interpretation of some of our new results.

Since the position of the P-site tRNA in the fMet-$tRNA_f^{Met}$–ribosome complex (Malhotra et al., 1998; Gabashvili et al., 2000) matched the tRNA position observed in the P site in the PRE and POST state complexes, the use of the map as a control in the computation of difference maps has the consequence that the mass corresponding to the P-site fMet-$tRNA_f^{Met}$ will always be subtracted. Nevertheless, the map was instrumental in determining the dipeptidyl-tRNA in the A site and the other low-occupancy, or short-lived, binding positions. We also analyzed the locations of negative masses in all difference maps. A negative difference mass occurs wherever the mass of the control (in this case, the fMet-$tRNA_f^{Met}$-bound ribosome) exceeds the mass of the complex analyzed. Within the intersubunit region, where tRNA binding is expected, the only negative mass observed was at the P site, probably caused by the higher occupancy of the P-site by fMet-$tRNA_f^{Met}$ in the subtracted ribosome (Malhotra et al., 1998; Agrawal et al., 1999c).

Difference Map Analysis

As pointed out earlier, two PRE complexes were analyzed to ascertain the A site position of acylated-tRNA (Phe-$tRNA^{Phe}$) and dipeptidyl-tRNA (fMet-Phe-$tRNA^{Phe}$), i.e., the position of tRNA before and after peptide bond formation. In the former case, the tRNA was directly visible (Fig. 1, a and c), whereas in the latter case, it was not, because of lower occupancy. The lower occupancy in the latter case, as pointed out earlier, could be due to a spontaneous translocation in a fraction of the PRE complexes, which could also account for the apparent occupancy of the E site in this complex. It is known that peptide bond formation stimulates spontaneous translocation (Bergemann and Nierhaus, 1983), but the reaction conditions for the PRE complex with the dipeptidyl-tRNA were chosen to minimize this process. Indeed, the biochemical characterization of the complex using the puromycin reaction revealed no significant translocation of the dipeptidyl-tRNA from the A to the P site (see Materials and Methods). A

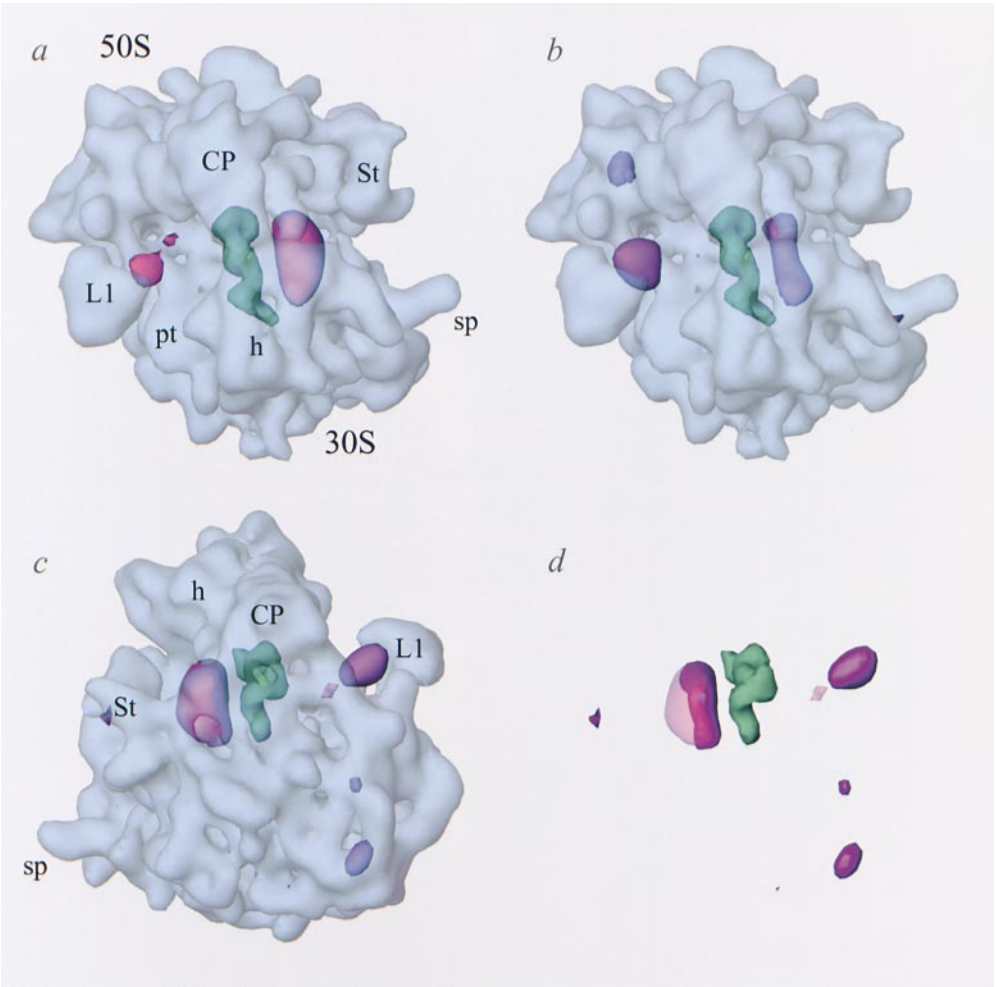

Figure 2. Difference maps, obtained by subtracting the 3D map of the fMet-$tRNA_f^{Met}$–70S ribosome complex (Malhotra et al., 1998) from those of the two PRE complexes, superimposed on the 15-Å resolution map of the ribosome (semitransparent blue). The ribosome is shown in a top view, with the 30S subunit below the 50S subunit. a, PRE complex containing Phe-$tRNA^{Phe}$ (pink) at the A site and deacylated $tRNA^{Phe}$ (green) at the P site, i.e., corresponding to the PRE complex shown in Fig. 1 c. b, PRE complex containing dipeptidyl tRNA (fMet-Phe-$tRNA^{Phe}$; violet) at the A site and deacylated $tRNA_f^{Met}$ (green) at the P site. c, The two difference maps superimposed with transparent pink. The 70S ribosome is viewed from the 50S-solvent side to indicate the shift in the position of the CCA half of the dipeptidyl tRNA towards the P-site tRNA. d, same as in c, but with the ribosome removed for clarity. The subtracted cryo-EM density corresponding to the P-site tRNA has been pasted in afterwards (green). For this, we have used the density due to fMet-$tRNA_f^{Met}$ (Gabashvili et al., 2000), which also carries an additional, inseparable mass on its anticodon end. As pointed out in the text, the mass of densities seen on the L1 side of the P-site tRNA (green) in both PRE complexes could be due to a conformational change in the L1 protein. CP, central protuberance; L1, L1-protein; St, L7/L12-stalk base; h, head; pt, platform; sp, spur.

possible way to explain this apparent paradox is to assume that the spontaneous translocation proceeds in two steps. In the first, fast step, the tRNAs move from the A and P sites to the P and E sites, whereas a slower conformational change of the ribosome or in the 3′-CCA end region of the dipeptidyl-tRNA is required to render the dipeptidyl-tRNA puromycin-reactive. This would mean that the majority of tRNAs were still in A site region, but corresponding density was averaged out in the 3D reconstruction, and thus not visible at normal thresholds. Time-resolved techniques of cryo-EM imaging might be used to test this hypothesis.

Because of the relatively low occupancy, a difference map had to be computed. To determine the differences in the binding positions of acylated-tRNA and dipeptidyl-tRNA, we computed difference maps by subtracting the 3D map of the P site-occupied tRNA–ribosome complex (Malhotra et al., 1998) from those of both PRE complexes (Fig. 2). Both difference maps show a strong mass of density on the L7/L12 stalk side of the P-site tRNA, which can readily be interpreted as A site-related tRNA-binding position of the ribosome (e.g., Zimmermann et al., 1990). These difference densities are superimposable on each other in most parts on the anticodon side (i.e., the 30S side) of the tRNA; whereas on the CCA arm side (i.e., the 50S side), the difference density corresponding to dipeptidyl-tRNA (Fig. 2 b) is shifted towards the CCA end of the P-site tRNA (Fig. 2, c and d). In addition, the PRE complex difference maps show an extra mass of density, which appears to be contributed by conformational change in the L1 protein. It should be noted that the 3D map of the fMet-tRNA$_f^{Met}$–ribosome complex (Malhotra et al., 1998) used for the computation of the difference map also has a mass in the E site region, which probably comes from contamination of deacylated tRNA$_f^{Met}$ in a fraction of the complex. Therefore, the difference maps (Fig. 2) do not show any E site-related density as seen in Fig. 1, a and c. The difference map computed by subtraction of the 3D map of the P site-occupied tRNA–ribosome complex from that of the POST complex yields a complex mass of density (not shown) on the L1 protein side of the P-site tRNA, but no mass on the L7/L12 side, showing that a complete translocation reaction was achieved.

The E site-related locations inferred from the POST complexes are different from the one identified in the previous study (Agrawal et al., 1996), where the E-site tRNA was shown to cling to the L1 protein. The difference map in recent studies of a POST complex (Agrawal et al., 1999a, 2000) showed a smeared-out mass that overlaps with both the newly identified (Fig. 1 d) and, in part, with the originally identified (Agrawal et al., 1996) E sites. In the POST maps studied here, the E site-related binding position of tRNA is found between the P site and the previously identified E site position (Agrawal et al., 1996; Fig. 3). The latter site is found in all deacylated tRNA-binding experiments carried out under the conditions of the conventional buffer (high 10–15 mM Mg^{2+}, no polyamines; see Agrawal et al., 1999c). Since the mass is distinct from either of the P/E (Agrawal et al., 1999c), as well as the E site positions of tRNA in the POST complex and polysomes (Agrawal, R.K, S. Srivastava, and J. Frank, unpublished results), we distinguish it as the E2 site. Thus, we attribute the mass originally identified with a tRNA at the E site (Agrawal et al., 1996), also found in the polysomes at lower threshold (Agrawal, R.K., S. Srivastava, and J. Frank, unpublished results), to the E2 site. Of the two E site-related binding positions observed, we consider E2 as a low-occupancy, short-lived position, as this is observed only in difference maps (Fig. 3), in contrast to the E site, which evidently has high occupancy as it can be seen directly in the 3D maps (e.g., Fig. 1 d).

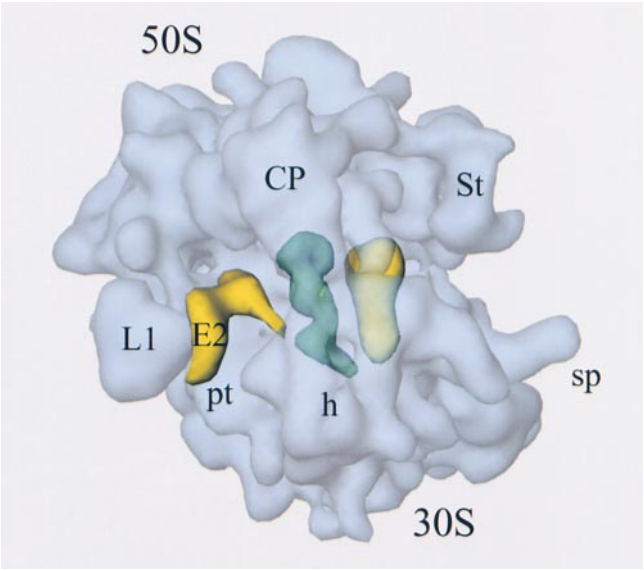

Figure 3. Difference maps obtained from a poly(U)-programmed ribosome–(tRNA^{Phe})$_3$ complex (adapted from Agrawal et al., 1999c) showing densities (yellow) corresponding to A, and overlapping P/E-, E-, and E2-site tRNAs. As in Fig. 2, the subtracted cryo-EM density corresponding to the fMet-tRNA$_f^{Met}$ has been pasted in afterwards (green). CP, central protuberance; L1, L1 protein; St, L7/L12-stalk base; h, head; pt, platform; sp, spur.

Comparison of Difference Masses Corresponding to tRNAs with the X-ray Structure

The next step was to find out the positions of the tRNAs by fitting the tRNA^{Phe} X-ray structure (Westhof et al., 1988) into the tRNA masses. To obtain an accurate fitting, we applied a 3D spherical mask, large enough to accommodate a tRNA (43-Å radius), around each discrete mass. This gave us a clear 3D view of the mass corresponding to one particular tRNA position at a time, and thus allowed us to obtain an unequivocal fitting of the X-ray structure in each case (Fig. 4).

For the A site location, overlapping difference masses from two different functional state complexes (before and after peptide bond formation, Fig. 2, a and b, respectively) were used. Fig. 4, a and b, show the fitting of the tRNA X-ray structure into the difference masses corresponding to the tRNA mass before and after peptide bond formation, respectively. Although the difference map obtained from the PRE complex containing Phe-tRNA^{Phe} at the A site shows the L-shaped feature for the fitting of the X-ray structure, extra room in its elbow region (Fig. 2 a) allows the possibility of wiggling movements of the X-ray struc-

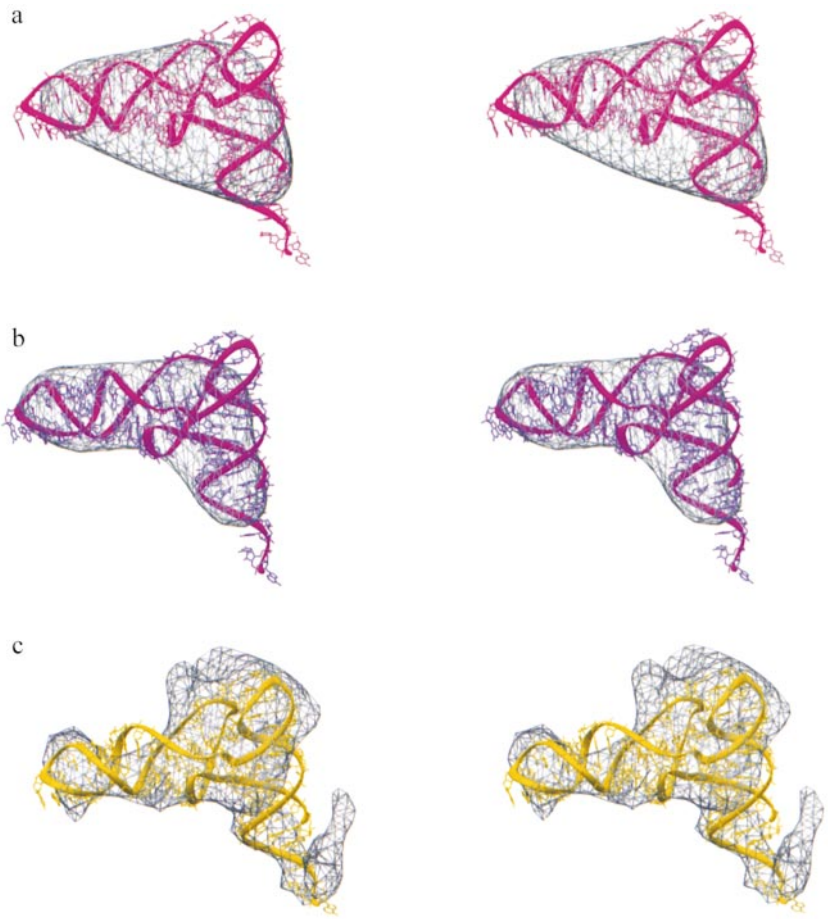

Figure 4. Stereo view representations to show the fitting of the X-ray structure of $tRNA^{Phe}$ into the various difference masses. The difference masses (gray wire-mesh) corresponding to the tRNA positions indicated were derived from the following complexes by applying a 3D spherical mask of 43 Å radius to the corresponding portions of the EM map and difference maps: a, A site (magenta), in the difference mass from the PRE complex containing Phe-$tRNA^{Phe}$ at the A site, as shown in Fig. 2 a; b, A_{Pep} state (violet), in the difference mass from the PRE complex containing dipeptidyl tRNA (fMet-Phe-$tRNA^{Phe}$) at the A site, as shown in Fig. 2 b; c, E site (yellow), in the mass from the POST complex map, as shown in Fig. 1, b and d.

ture in the direction of the L7/L12 stalk, further away from the elbow of the A_{Pep}-state tRNA (the position attained after the peptide bond formation) than that shown in Fig. 5 b. Since the position of the P-site tRNA in all the complexes analyzed in this study were the same as obtained in earlier studies (Malhotra et al., 1998; Agrawal et al., 1999a,c; Gabashvili et al., 2000), we do not present another fitting of the crystal structure into the corresponding density.

For the E site location, the $tRNA^{Phe}$ X-ray structure was fitted (Fig. 4 c) directly into the 3D map of the POST complex (Fig. 1, b and d). The tRNA position identified as the E2 site has been observed in three different complexes so far: two described in the previous studies (Agrawal et al., 1996, 1999c); and one in which a deacylated $tRNA^{Phe}$ was bound to the vacant 70S ribosome (Agrawal, R.K., R.A. Grassucci, and J. Frank, unpublished results). As pointed out before, polysomes also show a mass corresponding to a tRNA located at the E2 site, but with reduced density indicating occupancy in the range of 70% of that at the A site. We do not present the X-ray structure fitting for the E2-site tRNA, as its position is the same as presented earlier (Agrawal et al., 1996; Fig. 3). Moreover, it should be pointed out that, due to its close proximity with the L1 protein, which also moves upon tRNA binding (Agrawal, R.K., and J. Frank, unpublished results), the orientation of the E2-site tRNA (especially that of the CCA arm, as difference densities are also observed in that region in the PRE complexes, see Fig. 2) remains uncertain.

Relative Positions of tRNAs

The relative positions of tRNAs, as obtained by individual fits of the X-ray structure, are shown in Fig. 5. It is quite clear that the anticodons of A- and P-site tRNAs, and also of P- and E-site tRNAs, are in close mutual proximity. The distance between bases 37 of the A- and P-site tRNAs is 20 (± 3) Å, in good agreement with the fluorescence resonance energy transfer (FRET) data (Paulsen et al., 1983). The distance between the same bases of P- and E-site tRNAs is even smaller, 16 (± 3) Å. The CCA ends of A_{Pep}-state tRNA and the P-site tRNAs are also in close mutual proximity. Distances between the 3′-OH groups of nt 76 of A_{Pep}-state tRNA and the P-site tRNAs, and between P- and E-site tRNAs are 17 (± 3) Å and 60 (± 3) Å, respectively. The distance between the nt 76 of A site and A_{Pep}-state tRNAs is 10 (± 3) Å. The anticodon of the E2-site tRNA is far away from the anticodons of other tRNAs. The inter-tRNA–base distances obtained from this study and from earlier FRET data (Johnson et al., 1982; Paulsen et al., 1983) are strikingly similar. The angles between the equivalent planes of A site and A_{Pep}-state tRNAs is 8°. The angles between the equivalent planes of A_{Pep}-state

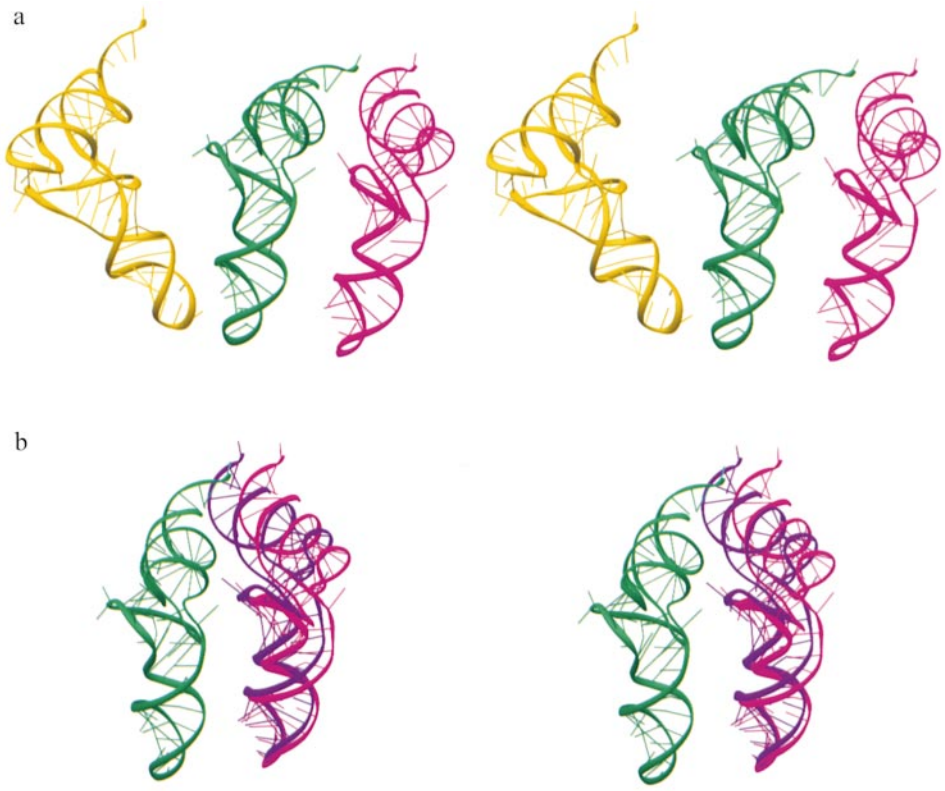

Figure 5. Stereo view representations showing the relative positions of tRNAs on the ribosome. a, A- (pink), P- (green), and E- (yellow) site tRNAs, as viewed from the top of the ribosome (ribosome not shown). b, A, A_{Pep} (violet), and P site. In both representations, the 30S subunit would be below the 50S subunit, as in Fig. 1.

and P-site tRNAs (39°), and between P- and E-site tRNAs (35°) are in the same range.

Discussion

The tRNA Positions in the Ribosomal Frame of Reference

The locations of the various tRNA-binding positions on the ribosomes have been derived by two different approaches: by directly fitting the extra mass of density in the 3D cryo-EM map (Fig. 1); and by computing difference maps (Figs. 2 and 3). The latter approach was essential when the occupancy of tRNA was low. For instance, in the A site, spontaneous translocation probably results in lower occupancy, and the occupancy achieved in vitro is generally <60%. This approach was also useful in identifying some of the presumably short-lived binding positions of the tRNA, e.g., the A_{Pep} and E2 positions. The locations of the tRNAs correspond to characteristic masses that allow a consistent fitting of a tRNA in each case. When we look at these fittings in the structural frame of reference provided by the intersubunit space of the 70S ribosome, they are at once convincing (Fig. 6). These positions clearly show that the ribosome has specific structural features that complement the structural features presented by its ligands, as in a lock and key arrangement (see Frank and Agrawal, 1998). The anticodons of the A_{Pep}-state, as well as A- and P-site tRNAs, are found in the immediate vicinity of the proposed mRNA entrance channel (Frank et al., 1995; Agrawal et al., 1996; Lata et al., 1996) passing through the neck of the 30S subunit. The anticodons of the A-site and A_{Pep}-state tRNAs are found on the shoulder side (Fig. 7 a), whereas that of the P-site tRNA is situated on the platform side of the channel (Fig. 7 c). Thus, the anticodons of A-site and A_{Pep}-state tRNAs are located near the 530-loop region (see Müller and Brimacombe, 1997) on the shoulder side and near the tip of helix 44 (Cate et al., 1999; Clemons et al., 1999; Gabashvili et al., 2000), the 1,400/1,500 region (on the P-site tRNA side) of the 16S rRNA. Whereas the anticodon ends of both A- and P-site tRNAs are located in the decoding region of the 30S subunit, their anticodon arms rest on helix 69 (highlighted by an asterisk in Fig. 7 b, see Gabashvili et al., 2000) of the 23S RNA. A major portion of the outer edge of the elbow region of both A-site and A_{Pep}-state tRNAs is situated between the L7/L12 stalk base and the long bridge (corresponding to helix 38 of the 23S RNA, and the tip of which was identified as bridge B1a; see Gabashvili et al., 2000) regions of the 50S subunit, with the elbow of the A-site tRNA shifted toward the L7/L12 stalk base side. Furthermore, the CCA ends of both A-site tRNA in the A_{Pep}-state and P-site tRNA are pointing (Malhotra et al., 1998) into the proposed polypeptide tunnel (Frank et al., 1995) present at the bottom of the interface canyon of the 50S subunit, where the peptidyltransferase center of the ribosome is located (marked by an asterisk in Fig. 7 d). A detailed description of the position of the P-site tRNA has been provided in an earlier article (Malhotra et al., 1998).

The E-site tRNA is positioned such that its anticodon end lies adjacent to the anticodon of the P-site tRNA (Fig. 6 b), touching the rim of the 30S subunit platform (Fig. 7 c), whereas the outer edge of its elbow touches the inner sur-

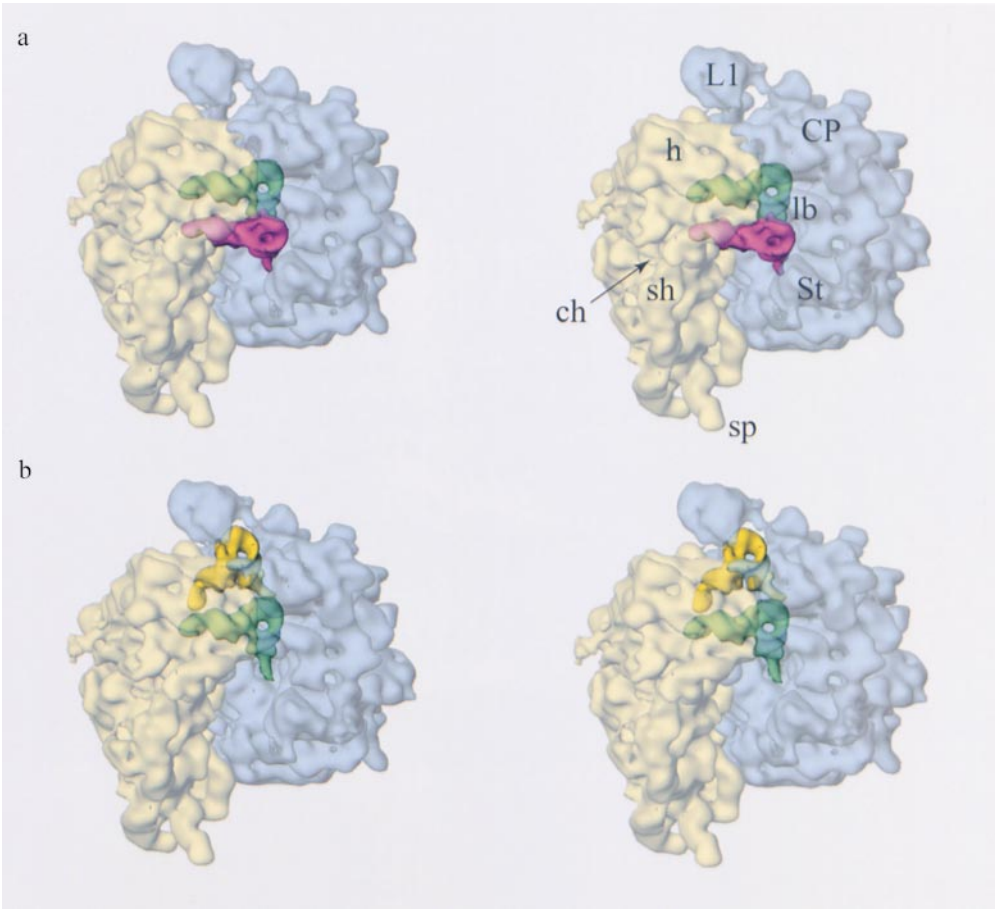

Figure 6. Stereo view representations of the fitted tRNAs placed into the 11.5-Å resolution 3D map of the 70S ribosome (Gabashvili et al., 2000). The crystal structure of $tRNA^{Phe}$, filtered to 5-Å resolution, was placed into the positions corresponding to A- (pink), P- (green), and E- (yellow) sites. The 70S ribosome is shown as a semitransparent surface, with the 30S subunit (yellow) on the left and the 50S subunit (blue) on the right. a, A- and P-site tRNAs in the PRE state. b, P- and E-site tRNAs in the POST state. lb, Long bridge, identified as helix 38 of the 23S RNA in an earlier study (Gabashvili et al., 2000); sh, shoulder region of the 30S subunit; ch, mRNA channel; CP, central protuberance; L1, L1 protein; St, L7/L12-stalk base; h, head; sp, spur.

face (an area between the stem and the globular portion) of the L1 protein protuberance (Figs. 6 b and 7 d). The CCA end of the E-site tRNA touches a region below the shoulder of the central protuberance, on the L1 protein side, in the interface canyon (Fig. 7 d). The overall orientation of the E-site tRNA is similar to that of an earlier identified P/E-state tRNA (Agrawal et al., 1999c), where the anticodon end of the tRNA overlaps with that of P-site tRNA. However, the tRNA in the E site has shifted toward the L1 protein protuberance as compared with its position in the P/E state. In the E2 site, the whole anticodon arm of the tRNA makes contact with the surface of the L1 protein protuberance facing the intersubunit space (Fig. 6 d). As pointed out earlier, because of the flexible nature of the L1 protein, the orientation of the tRNA at this site is uncertain. All tRNA-binding positions inferred in this study, in general, satisfy most of the cross-linking and chemical protection data (for review see Wower et al., 1993; Nagano and Nagano, 1997). These positions should provide important constraints for the 3D placements of the various cross-linked ribosomal proteins and rRNA segments on the ribosome in a given functional state.

Comparison to Previous Site Assignments

The A site position found here corresponds to that in our earlier analysis of a ribosome–poly(U)–$(tRNA^{Phe})_3$ complex (Agrawal et al., 1996), but has a different orientation; the present E2 site position virtually coincides with the position formerly identified as the E site in that work, whereas the present E site is observed with the POST state ribosome (Fig. 1, b and d). In an earlier study (Agrawal et al., 1996), the A-site tRNA was positioned such that its CCA end pointed towards the L1 protein. This position could be refined when the 70S–fMet-$tRNA_f^{Met}$ complex became available as a control to compute the difference map. Now, difference maps corresponding to the A-site tRNA show a well-defined, characteristic L-shaped structure, whose CCA end is directed towards the mouth of the proposed polypeptide tunnel in the interface canyon of the 50S subunit. The A and P site positions of Stark et al. (1997a) appear to be similar to the positions described here, whereas their E site does not correspond to any of E site-related positions (E or E2) we found in this study. In their placement, the E-site tRNA appears to penetrate into the platform and involve a large area of contact with the 30S subunit, in conflict with the previous results indicating that the E-site tRNA mainly has contacts with the 50S subunit (Kirillov et al., 1983; Gnirke and Nierhaus, 1986; Moazed and Noller, 1989a,b). It should also be noted that assignment of orientations to tRNAs in A and P sites in the study by Stark et al. (1997a) were guided by biochemical and tRNA–mRNA modeling data in addition to observed densities, since the latter covered only the anticodon arm of the corresponding tRNAs, providing no constraint for the orientation of the acceptor arm.

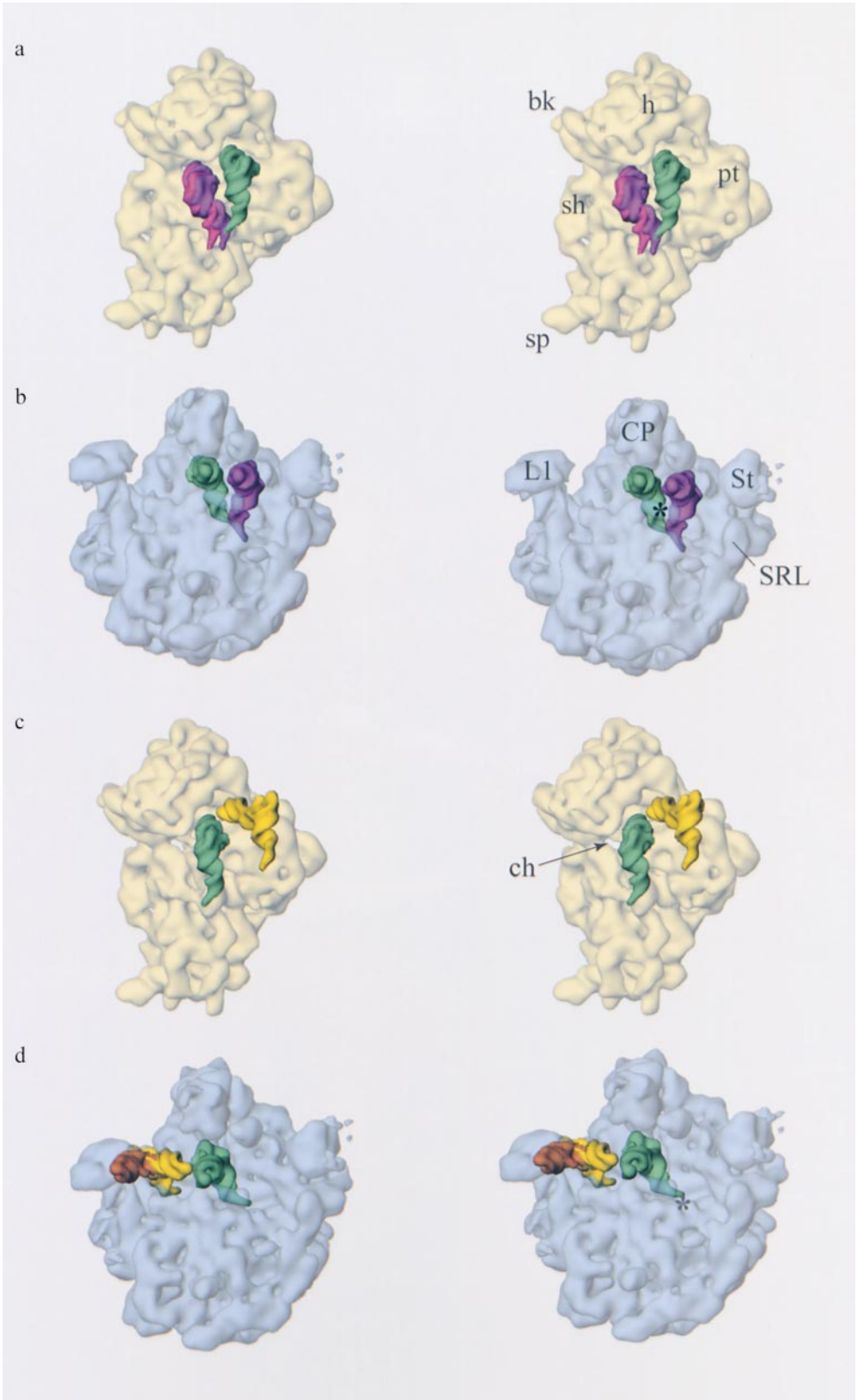

Figure 7. Stereo view representations of the tRNA positions on the ribosomal subunits (semitransparent), isolated from the 11.5-Å resolution 3D map of the 70S ribosome (Gabashvili et al., 2000). The ribosomal subunits, 30S (yellow) and 50S (blue), are shown from the subunit–subunit interface side. The crystal structure of $tRNA^{Phe}$ corresponding to A- (pink), A_{Pep}- (violet), P- (green), E- (yellow), and E2- (brown) site tRNAs was filtered to 5-Å resolution. a, A-, A_{Pep}-, and P-site tRNAs on the 30S subunit. b, A_{Pep}-state tRNA and P-site tRNAs on the 50S subunit. The asterisk (*) points to helix 69 of the 23S RNA (see text). c, P- and E-site tRNAs on the 30S subunit. The map has been slightly rotated (as compared with a) to make the mRNA channel visible. d, P-, E-, and E2-site tRNAs on the 50S subunit. The map has been slightly rotated (as compared with b) to show the relative position of anticodon ends in P, E, and E2 sites. The peptidyltransferase center, based on the position of the CCA ends of A_{Pep}-state and P-site tRNA, has been marked by an asterisk (*). The CCA arm of the tRNA at the E2 site is not shown as its orientation is uncertain (see text). bk, Beak of the 30S subunit head; SRL, α-sarcin/ricin loop region of the 23S RNA; sh, shoulder region of the 30S subunit; ch, mRNA channel; L1, L1 protein; St, L7/L12-stalk base; h, head; pt, platform; sp, spur.

After the completion of this work, the positions of A-, P-, and E-site tRNAs were also determined in X-ray maps of *T. thermophilus* 70S ribosomes (Cate et al., 1999), which appear in overall agreement with the binding positions of A-, P-, and E-site tRNA derived from this study. However, a close comparison of tRNA positions from the X-ray study (PDB submission #486D) with ours reveals some conflicts in fine details; e.g., the CCA end of the P-site tRNA in the

X-ray study was found shifted by ~10 Å toward the L1 side as compared with our position. This is due to the following obvious reasons: the X-ray work was carried out in very high Mg^{2+} concentration (>30 mM), and therefore, represents a condition that is far from physiological; in contrast to the X-ray work, we did not change the X-ray structure of tRNA for a better fit into our cryo-EM maps; and modeled tRNA structures used in the X-ray study were not stereochemically optimized. The formation of bonds between the ASL portions, which were modeled, and the rest of the tRNA is not possible.

From our results, and also from the results of Stark et al. (1997a), it appears that the P-site tRNA in PRE and POST states are in the same position. However, the resolution limit of our analysis does not permit a definite conclusion in this respect. The angle between equivalent surfaces of the tRNAs in P and E sites is such that it corresponds to the relative position of tRNAs in the A and P sites. The fact that the distance between the anticodons of P- and E-site tRNAs is comparable to that seen between A- and P-site tRNAs indicates that the tRNAs in the E site we identified may undergo codon–anticodon interaction in a similar way as those in the A or P sites. The proximity of the anticodons of A-, P-, and E-site tRNAs, and on that account, the stereochemical considerations of Lim (1997), are consistent with the allosteric three-site model (Nierhaus, 1990). The more recent α-ϵ model (Dabrowski et al., 1998) is based on the observation of unchanged mutual protection patterns of the tRNAs when going from the PRE to the POST state ribosome. Our results agree in part with the conclusion from these experiments, in that the relative position of the two tRNAs changes only little upon translocation. Here, we also observed an A_{Pep}-state, in which the CCA end of the A-site tRNA is shifted towards the CCA end of the P-site tRNA (Figs. 2, 5 b, and 7 a). For a more definitive conclusion on the spatial relation between the A- and A_{Pep}-state tRNAs, further investigation at higher resolution would be necessary, which is not an easy task because of the partial occupancy of these states. However, even the results at the present resolution make it clear that our A_{Pep}-state tRNA does not match the qualitative description of an A/P site postulated by Moazed and Noller (1989a), where the CCA half of the A-site tRNA occupies the P site position (see Noller et al., 1990). In an earlier study (Agrawal et al., 1999c), we reported a tRNA position corresponding to a hybrid P/E site, a site that is apparently specific for a single deacylated tRNA on a programmed ribosome and constitutes a predominant site under conventional, rather than polyamine, buffer conditions. It is not yet clear whether the P/E state we observed is a functional hybrid state (Moazed and Noller, 1989a) of the elongating ribosome.

The E and E2 Sites

The observation that the POST complex carries a highly occupied E site, but a weakly occupied E2 site, suggests that the E2 site is a short-lived tRNA-binding position. This site, whose occupation is observed in complexes prepared using deacylated tRNAs and high Mg^{2+} concentration (Agrawal et al., 1996, 1999c), might be a further station of the deacylated tRNA on the way out of the ribosome after the release from the E-site, and tRNA might be released from the E2 location before the E site is filled again in the next round of the elongation cycle (Fig. 8). The proximity of the anticodon ends of tRNA in the E site to that of P-site tRNA (Figs. 6 b and 7, c and d) suggests that codon–anticodon interaction is feasible at this stage. On the way from the E site to the E2 site, the anticodon end of the tRNA moves by a large distance (Fig. 7 d), which will disrupt its interaction with the codon downstream from that associated with the tRNA in the P site. The postulated codon–anticodon interaction at the E site (Nierhaus et al., 1998) therefore has to break before the tRNA can move to the E2 site position. The L1 protein, which makes contact with the elbow of the E-site tRNA (Fig. 6 b) and with most of the anticodon arm of the tRNA at the E2 position (Fig. 7 d), is considered nonessential for the functions of the ribosome, since mutants lacking L1 protein are known to be viable (Subramanian and Dabbs, 1980). However, as the growth of these mutants is slowed down by a factor of two, L1 might play a role assuring the optimal disposal of the tRNA after the release from the E site (Agrawal, R.K., and J. Frank, unpublished results).

The fact that the elbow regions of tRNAs at the E and E2 sites significantly overlap (Fig. 7 d) excludes the possibility that the two sites can be occupied simultaneously. This conclusion is also supported by the results derived from tRNA saturation experiments. It is well documented that programmed ribosomes can be saturated with three, but not four, tRNAs (Rheinberger et al., 1981; Grajevskaja et al., 1982; Lill et al., 1984). It is possible that the E2 site is only transiently occupied and binds tRNAs only with low affinity. The weakness of the E2 peak in polysomes (Agrawal, R.K., S. Srivastava, and J. Frank, unpublished results), indicates that the site is not a stable tRNA-binding site in vivo. It is conceivable that conventional buffer systems (i.e., without polyamines and with higher Mg^{2+} concentration) affect the ribosome structure in such a way that a tRNA leaving the ribosome is trapped in the E2 position.

Our E and E2 sites appear to be related to the E′ and E sites, respectively, of Robertson and coworkers (1986). According to their nomenclature, the E′ site is a codon–anticodon interaction-dependent, but short-lived tRNA position, from where the tRNA subsequently moves to an E site characterized by two properties: the anticodon can no longer interact with the codon; and tRNA at that site rapidly dissociates from the ribosome. Obviously, the site identified as E′ has all the features of the E site identified here, with the important exception that the tRNA in this E site could be directly observed, indicating relatively stable binding (for a discussion of this point, see Nierhaus et al., 1997). Likewise, the E site of Robertson et al. (1986) would correspond to the E2 site described in our work.

Dynamic Structural Features of the Ribosome in the Vicinity of tRNA-binding Sites

Superimposition of the 3D maps of PRE- and POST-state ribosomes reveal some features of the ribosome that could be related to functionally important conformational rearrangements. As compared with the PRE state, regions of shoulder and head of the 30S subunit shift toward the 50S

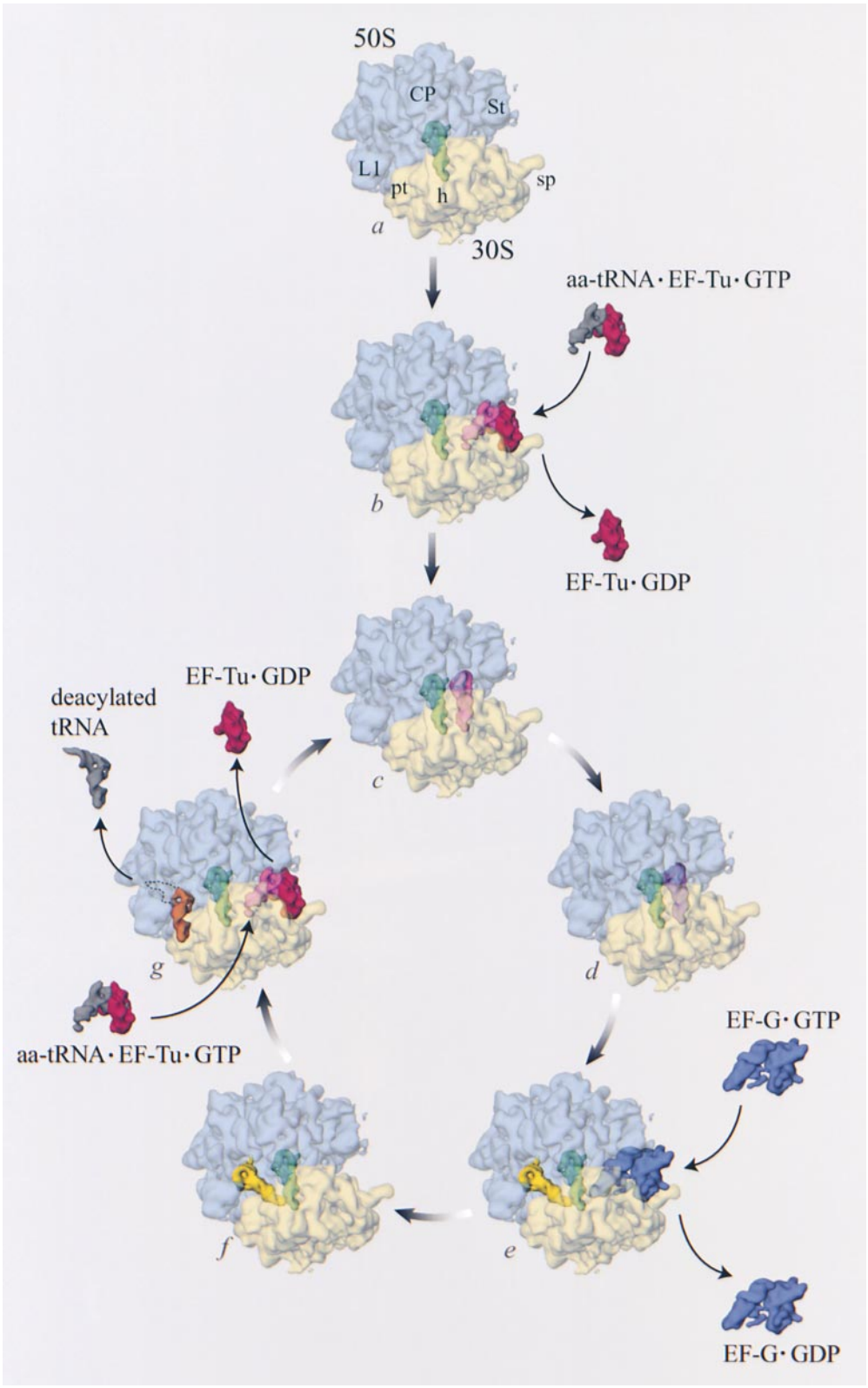

Figure 8. Various inferred positions of the tRNAs, overlaid on the 11.5-Å resolution 3D map of the ribosome to sketch out the elongation cycle. The transparent ribosome is shown in top view, with 30S subunit (yellow) below the 50S subunit (blue). Before entering into the elongation step, the 70S ribosome contains a tRNA (green) in the P site (a; Malhotra et al., 1998; Agrawal et al., 1999c; Gabashvili et al., 2000), which is approached by a ternary complex of aminoacyl-tRNA, EF-Tu, and GTP. The tRNA portion of the unbound ternary complex is presented in gray, the EF-Tu portion in red. The complex binds to the 70S initiation complex (b) in the A/T state (Moazed and Noller, 1989a). The binding position of the ternary complex to the ribosome has been obtained from a separate study (Agrawal, R.K., N. Burkhardt, R.A. Grassucci, K.H. Nierhaus, and J. Frank, unpublished results). The color of the tRNA portion of the ribosome-bound ternary complex is now shown in pink to identify the ribosomal A site. Similarly, in the subsequent panels, as the tRNA moves through the ribosome, its color coding is changed to identify a particular site. After GTP hydrolysis and release of the EF-Tu in its GDP conformation, tRNA is delivered to the A site. This results in the PRE state (c) of the ribosome with A (pink) and P (green) sites occupied. After spontaneous peptide bond formation, the CCA end of the A-site tRNA moves into the A_{Pep}-state (violet; d). At this stage, the EF-G–GTP complex (purple) binds to the ribosome (e) to facilitate translocation of tRNA from the A_{Pep}-state (violet) and P (green) sites to the P (green) and E (yellow) sites, respectively. The translocation reaction is induced by EF-G–dependent GTP hydrolyis accompanied by large transient conformational changes (not shown) in both EF-G and the ribosome (see Agrawal et al., 1999a, 2000; Frank and Agrawal, 2000). Release of EF-G in its GDP conformation leaves the ribosome in the POST state (f), which is ready to accept another molecule of the ternary complex in the vacated, overlapping binding site. We believe that during the start of the next cycle, i.e., upon binding of a new ternary complex in the A/T state (g), the E-site tRNA (yellow) moves further away from the P-site tRNA (green) to the E2 site (brown). The CCA arm of the E2-site tRNA is shown as dashed line, indicating that its orientation is uncertain (see text).

subunit, narrowing the gap between the two subunits on the side of the A site. Apparently, coordinated with this is the emergence of a structure that appears at the base of the stalk in POST complex (not shown), near the empty A site, where a portion of the A site-bound tRNA would be located in the PRE complex. This structure (shown clearly in Agrawal et al., 1999b) might be part of a blocking mechanism responsible for the low affinity of the A site in the POST-state ribosome. As such, it would only allow codon–anticodon interaction at the A site, but prevent other contacts of the ternary complex with the ribosome during the decoding process. Evidence for such a mechanism has been reported, and is thought to be of utmost importance for insuring the accuracy of the decoding process (Geigenmüller and Nierhaus, 1990; for review see Nierhaus 1993).

With the tRNA positions identified so far, along with the results of elongation factor binding (EF-Tu: Agrawal, R.K., N. Burkhardt, R.A. Grassucci, K.H. Nierhaus, and J. Frank, unpublished results; and EF-G: Agrawal et al., 1998, 1999a), we present the main sequence of events (without including the intermediate state, P/E) during the elongation cycle in Fig. 8. Our results offer a wealth of data on experimentally observed, genuine positions of the tRNA in biochemically defined ribosomal states. It is gratifying that the positions of A- and P-site tRNAs, which were inferred directly from the cryo-EM maps by fitting of the X-ray structure, without help from biochemical cross-linking or protection data, are in excellent agreement with distances inferred from FRET measurements.

We thank Amy Heagle for extensive help in some of the image processing and in the preparation of the illustrations, and Margaret Van Loock for help in preparing the ribbon diagrams.

This work was supported by the Deutsche Forschungsgemeinschaft, grant Ni 174/8-1 (to K.H. Nierhaus), by the National Institutes of Health grants 1R37 GM 29169 and 1R01 GM 55440 (to J. Frank), and by the National Science Foundation grant BIR 9219043 (to J. Frank).

Submitted: 26 April 2000
Revised: 13 June 2000
Accepted: 16 June 2000

References

Agrawal, R.K., and D.P. Burma. 1996. Sites of ribosomal RNAs involved in the subunit association of tight and loose couple ribosomes. *J. Biol. Chem*. 271: 21285–21291.

Agrawal, R.K., and J. Frank. 1999. Structural studies of translational apparatus. *Curr. Opin. Struct. Biol.* 9:215–221.

Agrawal, R.K., P. Penczek, R.A. Grassucci, Y. Li, A. Leith, K.H. Nierhaus, and J. Frank. 1996. Direct visualization of A-, P-, and E-site transfer RNAs in the *Escherichia coli* ribosome. *Science.* 271:1000–1002.

Agrawal, R.K., P. Penczek, R.A. Grassucci, and J. Frank. 1998. Visualization of elongation factor G on the *Escherichia coli* ribosome: the mechanism of translocation. *Proc. Natl. Acad. Sci. USA*. 95:6134–6138.

Agrawal, R.K., A.B. Heagle, P. Penczek, R.A. Grassucci, and J. Frank. 1999a. EF-G-dependent GTP hydrolysis induces translocation accompanied by large conformational changes in the 70S ribosome. *Nat. Struct. Biol.* 6:643–647.

Agrawal, R.K., K.R. Lata, and J. Frank. 1999b. Conformational variability in *E. coli* 70S ribosome as revealed by 3D cryo-electron microscopy. *Intl. J. Biochem. Cell Biol.* 31:243–254.

Agrawal, R.K., P. Penczek, R.A. Grassucci, N. Burkhardt, K.H. Nierhaus, and J. Frank. 1999c. Effect of buffer conditions on the position of tRNA on the 70S ribosome as visualized by cryo-electron microscopy. *J. Biol. Chem*. 274: 8723–8729.

Agrawal, R.K., A.B. Heagle, and J. Frank. 2000. Studies of elongation factor-G–dependent tRNA translocation by three-dimensional cryo-electron microscopy. *In* The Ribosome: Structure, Function, Antibiotics, and Cellular Interactions. R.A. Garrett, S.R. Douthwaite, A. Liljas, A.T. Matheson, P.B. Moore, and H.F. Noller, editors. American Society for Microbiology Press, Washington, DC. 53–62.

Bergemann, K., and K.H. Nierhaus. 1983. Spontaneous, elongation factor G independent translocation of *Escherichia coli* ribosomes. *J. Biol. Chem*. 258: 15105–15113.

Bommer, U., N. Burkhardt, R. Jünemann, C.M.T. Spahn, F.J. Triana-Alonso, and K.H. Nierhaus. 1997. Ribosomes and polysomes. *In* Subcellular Fractionation: A Practical Approach. J. Graham and D. Rickwood, editors. IRL Press, Washington, DC. 271–301.

Brimacombe, R. 1995. The structure of ribosomal RNA: a three-dimensional jigsaw puzzle. *Eur. J. Biochem*. 230:365–383.

Cate, J.H., M.M. Yushupov, G.Z. Yushupova, T.N. Earnest, and H.F. Noller. 1999. X-ray crystal structures of 70S ribosome functional complexes. *Science.* 285:2095–2104.

Clemons, W.M. Jr., J.L.C. May, B.T. Wimberly, J.P. McCutcheon, M. Capel, and V. Ramakrishnan. 1999. Structure of a bacterial 30S ribosomal subunit at 5.5 Å resolution. *Nature.* 400:833–840.

Dabrowski, M., C.M. Spahn, M.A. Schafer, S. Patzke, and K.H. Nierhaus. 1998. Protection patterns of tRNAs do not change during ribosomal translocation. *J. Biol. Chem*. 273:32793–32800.

Dubochet, J., M. Adrian, J.J. Chang, J.C. Homo, J. Lepault, A.W. McDonnall, and P. Schultz. 1988. Cryo-electron microscopy of vitrified specimens. *Rev. Biophys.* 21:129–228.

Frank, J. 1998. The ribosome-structure and functional ligand-binding experiments using cryo-electron microscopy. *J. Struct. Biol.* 124:142–150.

Frank, J., and R.K. Agrawal. 1998. The movement of tRNA through the ribosome. *Biophys. J.* 74:589–594.

Frank, J., and R.K. Agrawal. 2000. A ratchet-like intersubunit reorganization of ribosome during translocation. *Nature.* 406:318–322.

Frank, J., J. Zhu, P. Penczek, Y. Li, S. Srivastava, A. Verschoor, M. Radermacher, R. Grassucci, R.K. Lata, and R.K. Agrawal. 1995. A model of protein synthesis based on cryo-electron microscopy of the *E. coli* ribosome. *Nature.* 376:441–444.

Gabashvili, I.S., R.K. Agrawal, C.M.T. Spahn, R. Grassucci, D. Svergun, J. Frank and P. Penczek. 2000. Solution structure of *Escherichia coli* 70S ribosome at 11.5 Å resolution. *Cell.* 100:537–549.

Geigenmüller, U., and K.H. Nierhaus. 1990. Significance of the third tRNA binding site, E site, on *E. coli* ribosomes for the accuracy of translation: an occupied E site prevents the binding of non-cognate aminoacyl-tRNA to the A site. *EMBO (Eur. Mol. Biol. Organ.) J.* 9:4527–4533.

Ghosh, N., and P.B. Moore. 1979. An investigation of the conformational properties of ribosomes using N-ethylmaleimide as a probe. *Eur. J. Biochem*. 93: 147–156.

Gnirke, A., and K.H. Nierhaus. 1986. tRNA binding sites on the subunits of *Escherichia coli* ribosomes. *J. Biol. Chem*. 261:14506–14514.

Grajevskaja, R.A., Y.N. Ivanov, and E.M. Saminsky. 1982. 70S ribosomes of *Escherichia coli* have an additional site for deacylated tRNA binding. *Eur. J. Biochem*. 128:47–52.

Green, R., and H.F. Noller. 1997. Ribosomes and translation. *Ann. Rev. Biochem*. 66:679–716.

Green, R., and J.D. Puglisi. 1999. The ribosome revealed. *Nat. Struct. Biol.* 6:999–1003.

Johnson, A.E., H.J. Adkins, E.A. Matthews, and C.R. Cantor. 1982. Distance moved by transfer RNA during translocation from the A site to the P site on the ribosome. *J. Mol. Biol.* 156:113–140.

Kirillov, S.V., E.M. Makarov, and Y.P. Semenkov. 1983. Quantitative study of deacylated tRNA with *Escherichia coli* ribosomes: role of 50S subunits in formation of the E site. *FEBS Lett.* 157:91–94.

Lata, K.R., R.K. Agrawal, P. Penczek, R. Grassucci, J. Zhu, and J. Frank. 1996. Three-dimensional reconstruction of the *Escherichia coli* 30S ribosomal subunit in ice. *J. Mol. Biol.* 262:43–52.

Lill, R., J.M. Robertson, and W. Wintermeyer. 1984. tRNA binding sites of ribosomes from *Escherichia coli. Biochemistry*. 23:6710–6717.

Lill, R., J.M. Robertson, and W. Wintermeyer. 1986. Affinities of tRNA binding sites of ribosomes from *E. coli. Biochemistry*. 25:3245–3255.

Lim, V.I. 1997. Analysis of interactions between the codon–anticodon duplexes within the ribosome: their role in translation. *J. Mol. Biol.* 266:877–890.

Malhotra, A., P. Penczek, R.K. Agrawal, I.S. Gabashvili, R.A. Grassucci, N. Burkhardt, R. Jünemann, K.H. Nierhaus, and J. Frank. 1998. *E. coli* 70S ribosome at 15 Å resolution by cryo-electron microscopy: Localization of fMet-tRNA$_f^{Met}$ and fitting of L1 protein. *J. Mol. Biol.* 280:103–116.

Mesters, J.R., A.P. Potapov, J.M. de Graaf, and B. Kraal. 1994. Synergism between the GTPase activities of EF-Tu–GTP and EF-G–GTP on empty ribosomes: Elongation factors as stimulators of the ribosomal oscillation between two conformations. *J. Mol. Biol.* 242:644–654.

Moazed, D., and H.F. Noller. 1989a. Intermediate states in the movement of transfer RNA in the ribosome. *Nature.* 342:142–148.

Moazed, D., and H.F. Noller. 1989b. Interaction of tRNA with 23S RNA in ribosomal A, P and E sites. *Cell.* 57:585–597.

Müller, F., and R. Brimacombe. 1997. A new model for the three-dimensional folding of *Escherichia coli* 16S ribosomal RNA. II. The RNA–protein interaction data. *J. Mol. Biol.* 271:545–565.

Nagano, K., and N. Nagano. 1997. Transfer RNA docking pair model in the ribosomal pre- and post-translocational states. *Nucleic Acids Res.* 25:1254–1264.

Nierhaus, K.H. 1990. The allosteric three site model for the ribosomal elongation cycle: features and future. *Biochemistry.* 29:4997–5008.

Nierhaus, K.H. 1993. Solution of the ribosome riddle: how the ribosome selects the correct aminoacyl-tRNA out of 41 similar contestants. *Mol. Microbiol.*

9:661–669.

Nierhaus, K.H., R. Jünemann, and C.M.T. Spahn. 1997. Are the current three-site models valid description of the elongation cycle? *Proc. Natl. Acad. Sci. USA*. 94:10499–10500.

Nierhaus, K.H., J. Wadzack, N. Burkhardt, R. Jünemann, W. Meerwinck, R. Willumeit, and H.B. Stuhrmann. 1998. Structure of the elongating ribosome: arrangement of the two tRNAs before and after translocation. *Proc. Natl. Acad. Sci. USA*. 95:945–950.

Noller, H.F., D. Moazed, S. Stern, T. Powers, P.N. Allen, J.M. Robertson, B. Weiser, and K. Triman. 1990. Structure of rRNA and its functional interactions in translation. *In* The Ribosome: Structure, Function, and Evolution. W.E. Hill, A. Dahlberg, R.A. Garrett, P.B. Moore, D. Schlessinger, and J.R. Warner, editors. American Society for Microbiology Press, Washington, DC. 73–92.

Orlova, E.V., P. Dube, J.R. Harris, E. Beckman, F. Zemlin, J. Markl, and M. van Heel. 1997. Structure of keyhole limpet hemocyanin type 1 (KHL1) at 15 Å resolution by electron cryomicroscopy and angular reconstruction. *J. Mol. Biol.* 271:417–437.

Paulsen, H., J.M. Robertson, and W. Wintermeyer. 1983. Topological arrangement of two transfer RNAs on the ribosome: fluorescence energy transfer measurements between A and P site-bound $tRNA^{Phe}$. *J. Mol. Biol.* 167:411–426.

Penczek, P., R.A. Grassucci, and J. Frank. 1994. The ribosome at improved resolution: new techniques for merging and orientation refinement in 3D cryo-electron microscopy of biological particles. *Ultramicroscopy*. 53:251–270.

Rheinberger, H.-J., H. Sternbach, and K.H. Nierhaus. 1981. Three tRNA binding sites on *E. coli* ribosome. *Proc. Natl. Acad. Sci. USA*. 76:5310–5314.

Robertson, J.M., H. Paulsen, and W. Wintermeyer. 1986. Pre-steady-state kinetics of ribosomal translocation. *J. Mol. Biol.* 192:351–360.

Schilling-Bartetzko, S., A. Bartetzko, and K.H. Nierhaus. 1992. Kinetic and thermodynamic parameters for tRNA binding to the ribosome and for the translocation reaction. *J. Biol. Chem*. 267:4703–4712.

Spahn, C.M., and K.H. Nierhaus. 1998. Models of the elongation cycle: an evaluation. *Biol. Chem*. 379:753–772.

Stark, H., E.V. Orlova, J. Rinke-Appel, N. Jünke, F. Mueller, M. Rodnina, W. Wintermeyer, R. Brimacombe, and M. van Heel. 1997a. Arrangement of tRNAs in pre- and posttranslational ribosomes revealed by electron cryomicroscopy. *Cell.* 88:19–28.

Stark, H., M. Rodnina, J. Rinke-Appel, R. Brimacombe, W. Wintermeyer, and M. van Heel. 1997b. Visualization of elongation factor Tu on the *Escherichia coli* ribosome. *Nature.* 389:403–406.

Stöffler-Meilicke, M., and G. Stöffler. 1990. Topography of the ribosomal proteins from *Escherichia coli* within the intact subunits as determined by immunoelectron microscopy and protein–protein cross-linking. *In* The Ribosome: Structure, Function, and Evolution. W.E. Hill, A. Dahlberg, R.A. Garrett, P.B. Moore, D. Schlessinger, and J.R. Warner, editors. American Society for Microbiology Press, Washington, DC. 123–133.

Subramanian, A.R., and E.R. Dabbs. 1980. Functional studies on ribosome lacking protein L1 from *Escherichia coli. Eur. J. Biochem*. 112:425–430.

Triana-Alonso, F.J., M. Dabrowski, J. Wadzack, and K.H. Nierhaus. 1995. Self-coded 3′-extension of run-off transcripts produces aberrant products during *in vitro* transcription with T7 RNA polymerase. *J. Biol. Chem*. 270:6298–6307.

Wagenknecht, T., R. Grassucci, and J. Frank. 1988. Electron microscopy and computer image averaging of ice-embedded large ribosomal subunits from *Escherichia coli. J. Mol. Biol.* 199:137–145.

Westhof, E., P. Dumas, and D. Moras. 1988. Restrained refinement of two crystalline forms of yeast aspartic acid and phenylalanine transfer RNA crystals. *Acta Crystallogr. Sect. A*. 44:112–123.

Wilson, K.S., and H.F. Noller. 1998. Molecular movement inside the translational engine. *Cell.* 92:337–349.

Wower, J., L.A. Sylvers, K.V. Rosen, S.S. Hixson, and R.A. Zimmermann. 1993. A model of the tRNA binding sites on the *Escherichia coli* ribosome. *In* The Translational Apparatus: Structure, Function, Regulation, and Evolution. K.H. Nierhaus, F. Franceschi, A.R. Subramanian, V.A. Erdmann, and B. Wittmann-Liebold, editors. Plenum Press, New York. 455–464.

Zhu, J., P.A. Penczek, R. Schröder, and J. Frank. 1997. Three-dimensional reconstruction with contrast transfer function correction from energy-filtered cryoelectron micrographs: procedure and application to the 70S *Escherichia coli* ribosome. *J. Struct. Biol.* 118:197–219.

Zimmermann, R.A., C.L. Thomas, and J. Wower. 1990. Structure and function of rRNA in the decoding domain and the peptidyltransferase center. *In* The Ribosomes: Structure, Function and Evolution. W.E. Hill, A. Dahlberg, R.A. Garrett, P.B. Moore, D. Schlessinger, and R. Warner, editors. American Society for Microbiology Press, Washington, DC. 331–347.